Journal of Crystal Growth 311 (2009) 1206–1211

Contents lists available at ScienceDirect

Journal of Crystal Growth

journal homepage: www.elsevier.com/locate/jcrysgro

Role of substrate in the surface diffusion and kinetic roughening of nanocrystallised nickel electrodeposits

L. Nzoghe-Mendome [a], A. Aloufy [c], J. Ebothé [a,*], M. El Messiry [c], D. Hui [b]

[a] Laboratoire de Microscopies & d'Etude de Nanostructures, E.A. no. 3799, UFR Sciences, Université de Reims, B.P. 138, 21 rue Clément Ader, 51685 Reims cedex 02, France
[b] University of New Orleans, Department of Mechanical Engineering, New Orleans, LA 70148, USA
[c] Alexandria University, New Advanced Materials & Nanotechnology Center, Faculty of Engineering, Textile & Materials Engineering Department, 21544 Alexandria, Egypt

ARTICLE INFO

Article history:
Received 7 November 2008
Accepted 18 November 2008
Communicated by P. Rudolph
Available online 27 November 2008

PACS:
68.35 Ct
68.35 Fx
81.15 Pq
81.15.Aa

Keywords:
A1. Growth models
A1. Roughening
A1. Substrate
A2. Electrochemical growth
B1. Metals
B1. Nanomaterials

ABSTRACT

The surface growth and roughening of nano-crystallised Ni electrodeposits prepared at the same conditions have been studied on Cu, Au and ITO substrates. The Ni films obtained are characterised by the same face-centred cubic structure with a texture affected by the substrate chemical nature. Practically, the same small-sized grains of 83 nm mean height depicting a statistical mono-mode feature grow on Cu. A three-modal feature corresponding to the biggest and compact crystallites of 335, 368 and 400 nm mean height is obtained with Au. Two typical modes, respectively, linked to isolated big crystallites of 343 nm mean height and large zones of small grains of 170 nm height, result from the ITO effect. The surface transport properties of Ni ad-atoms on each substrate have been studied from the theoretical approach including the film global roughness measured by AFM. It is shown that the ad-atom diffusion coefficients (D_s) ranged in the interval 10^{-10}–10^{-9} cm^2 s^{-1} are greatly affected by the non-equilibrium conditions of the film formation. Cu and ITO, respectively, lead to Λ_s=11.92 and 14.30 nm, while the higher D_s value and diffusion length Λ_s=37.32 nm are obtained with Au substrate.

1. Introduction

Formerly, metallic supports were the only substrates used in cathodic formation of electrodeposits. Nowadays, various exotic conductive materials [1–3] are also experimented. Usually, their influence is reported from the study of the deposition method effects so that only the film morphology can be examined in that case [4]. Ultimately, their chemical nature plays a crucial role in the growth of nano-crystallised films [5] as it directly affects the surface diffusion of the ad-atoms and the film's kinetic roughening process. The control of each one of these two points and the understanding of their link seem the necessary steps to handle for optimising the global feature of this particular type of films for the specific needs of various application fields. The requirement of having mesoscopic thickness values and surface irregularities limited to some tenths root-mean-square (*rms*) roughness could be more easily achieved thereby. In that frame, we previously modelled a relationship between topography and transport parameters and tested it to the study of the chemical composition [6] and current density [7] effects in the growth of nickel and alloys electrodeposits. In the present work, the substrate material is examined with the same objective of clarifying in a better way the important role of this deposition parameter. A practical substrate as indium tin oxide (ITO) extensively used nowadays is here compared to the classical metallic materials as copper and gold. The growth of nickel films is carried out by chrono-amperometry away from the hydrogen reduction disturbance as it has been recently reported [7]. The details on the experimental procedure are fully given in Section 2, where the investigated substrates, the film preparation conditions and the sample characterisation techniques are presented. The results obtained are proposed and discussed in Section 3 on the basis of the link between the surface transport properties and the topography parameters. The specific effects of each substrate are then evaluated and compared.

2. Experimental procedure

2.1. Preparation and characteristics of the substrate materials

The substrates of the present work have different origins. Copper plates are made of 99.99% material purity whose surfaces are carefully polished on rotating abrasive disks of decreasing size. This mechanical procedure is ended by the use of a 0.1 μm

*Corresponding author. Tel.: +33 3 26 05 19 01; fax: +33 3 26 05 19 00.
E-mail address: jean.ebothe@univ-reims.fr (J. Ebothé).

0022-0248/$ - see front matter © 2008 Elsevier B.V. All rights reserved.
doi:10.1016/j.jcrysgro.2008.11.073

diamond powder leading to a bright surface feature. ITO-coated glasses are highly conductive and transparent specimens of Diamond Coatings Limited Company. Gold substrates are home-made films evaporated on chrome-coated glass slides under a pressure of 10^{-5} Torr. These slides are pre-heated at 58 °C prior to evaporation in order to ensure a good gold adherence. The smoothness of these substrates, expressed in terms of *rms* roughness, remains of the same order of magnitude namely σ(Cu)=7.01 nm; σ(Au)=3.22 nm and σ(ITO)=1.80 nm, knowing that ITO has a sheet resistivity of 22.5 Ω/square. As shown in Ref. [5], Cu and Au are both polycrystalline films of face-centred cubic (fcc) structure with Au greatly marked by the [111] preferred growth orientation while ITO is amorphous.

2.2. Deposition conditions and characterization techniques

The Ni samples are prepared in a three-electrode cell system from a 1 M $Ni(SO_4)_2$ aqueous electrolyte (pH=3.5) made of a FLUKA product (purity > 99%). A stationary substrate of 0.5 cm^2 area is used as the working electrode, and a saturated calomel electrode (SCE) serves as the potential reference. This cell is kept in a constant temperature T=323 K, and the chrono-amperometry experiments are performed with a radiometer PGP 201 potentiostat at a fixed current density J=22 mA cm^{-2}. This current density has been selected as it markedly enhances the specific influence of each substrate.

Once formed, the Ni electrodeposit thickness is measured from a commercial STRATAGem (SAM*x* France) software associated with X-ray microanalysis as described in Refs. [8,9]. Accordingly, the Ni electrodeposit thickness is evaluated referring to the X-ray intensity of the substrate material elements. Their structure is analysed from a BRUCKER D8 ADVANCE X-ray set using a Cu(Kα) irradiation. Their nanoscaled topography measurements are carried out with a standalone SMENA atomic force microscope (AFM) operating in a constant contact force mode. The AFM images and the topography parameters of the film surface are collected in ambient atmosphere. Every image is digitised into (512 × 512) pixels with a scanning frequency of about 1 Hz. The cantilever is composed of a commercial Si_3N_4 tip of approximately 50 nm apex radius bearing a 0.06 N m^{-1} spring coefficient. The local topography parameters are measured from nearly 15 zones of the same film surface, the statistic being improved by repeating the same procedure to 10 samples deposited under strictly the same conditions. These parameters are hereby supplied with an estimated error less than 10%. One points out that these measurements are reliable only with fully coalesced films. This condition is achieved from a minimal Ni film thickness of 50 nm as this value entirely covered the surface irregularities of bare substrates.

3. Results and discussion

The specific chemical nature of each substrate leads to different interface properties that directly affect both the material growth process including the Ni ad-atoms surface transport and the final microstructure of the electrodeposits obtained. Obviously, the growth steps can also evolve with the increase in the material quantity on one substrate. Consequently, the same Ni film thickness of 1 μm is retained in this section for our proposed comparative study.

3.1. Microstructure and surface morphology of Ni electrodeposits

The experimental X-ray diffractograms of Fig. 1 show that Ni films grow in the fcc structure, regardless of the substrate used. Referring to the Ni powder X-ray feature, one notes in Fig. 1(a and c) that ITO and Au substrates both lead to polycrystalline films of (111) preferred growth orientation, the film on ITO depicting more intensive (200), (220) and (311) peaks. One sees in Fig. 1(b) that the worse Ni-textured sample is supplied by Cu substrate as the (111), (200) and (220) peaks obtained here have nearly the same intensity. The change induced by the substrate is also observed in the Ni film surface morphology, as it appears in the 3D-AFM images of Fig. 2. Actually, the Ni crystallites on Au and ITO mostly exhibit a conic shape regardless of their size, the main difference appearing in the repartition of the small and big crystallites all over the film surface. The morphology of Fig. 2(b) obtained with Au results from the biggest crystallites having a mean diameter S(Au) ≈ 520 nm. The surface of Fig. 2(c) related to ITO is characterised by isolated big crystallites of $S(ITO)_1 \approx 430$ nm diameter that are quite separated from each other by large zones made of small grains of $S(ITO)_2 \approx 215$ nm diameter. The sample obtained with copper exhibits in Fig. 2(a) a more uniform surface feature of the smallest nanocrystallites having nearly the same size S(Cu) ≈ 325 nm that leads to the highest compactness degree. The histograms of the Ni film's surface morphology on the investigated substrates of Fig. 3 give the height repartition of the formed grains. The result of Fig. 3(a) with Cu substrate concurs with the visual observation of the morphology of the AFM image as it denotes only one statistical mode of the mean grain height h_0 (Cu) ≈ 83 nm given. The Ni grains on Au lead to a tri-modal feature as portrayed in Fig. 3(c), the related mean grain heights h_0(Au) ≈ 335 nm; h'(Au) ≈ 368 nm; h''(Au) ≈ 400 nm being very close to each other. The marked difference between small grains and nano-crystallites observed in Fig. 2(c) with ITO is also depicted here with the tri-modal histogram of Fig. 3(b) where nano-crystallites have a mean grain height h''(ITO) ≈ 345 nm in great contrast with the value h_0 (ITO) ≈ 170 nm of the smallest grains, where an intermediate mode corresponding to h'(ITO) ≈ 240 nm appears.

3.2. Topography of the Ni nano-crystallised films

The difference of surface morphology due to the substrate prompts to examine the film's topography aspects. As mentioned elsewhere, the Family–Vicsek approach satisfactorily describes the surface growth under non-equilibrium conditions [10,11]. One knows that electrodeposition mostly belongs to this growth category [6,12]. The model is based on the scaling behaviour of the interface width or local *rms* surface roughness (σ), as already reported elsewhere [5,13,14]. This topography parameter is

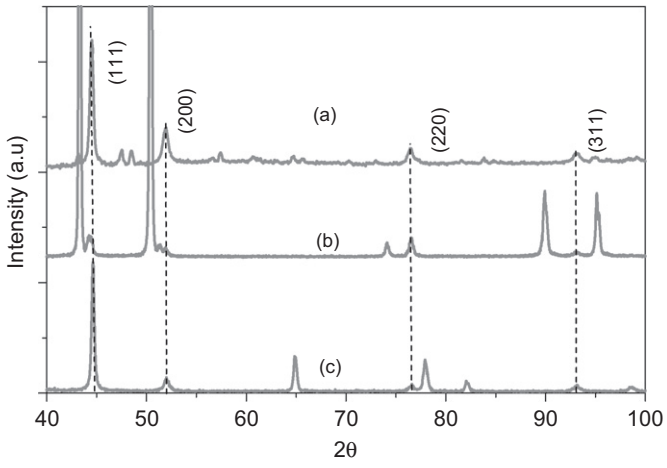

Fig. 1. X-ray diffractograms of the Ni nano-crystallised electrodeposits of 1 μm thickness obtained on each investigated substrates: (a) ITO, (b) Cu, and (c) Au.

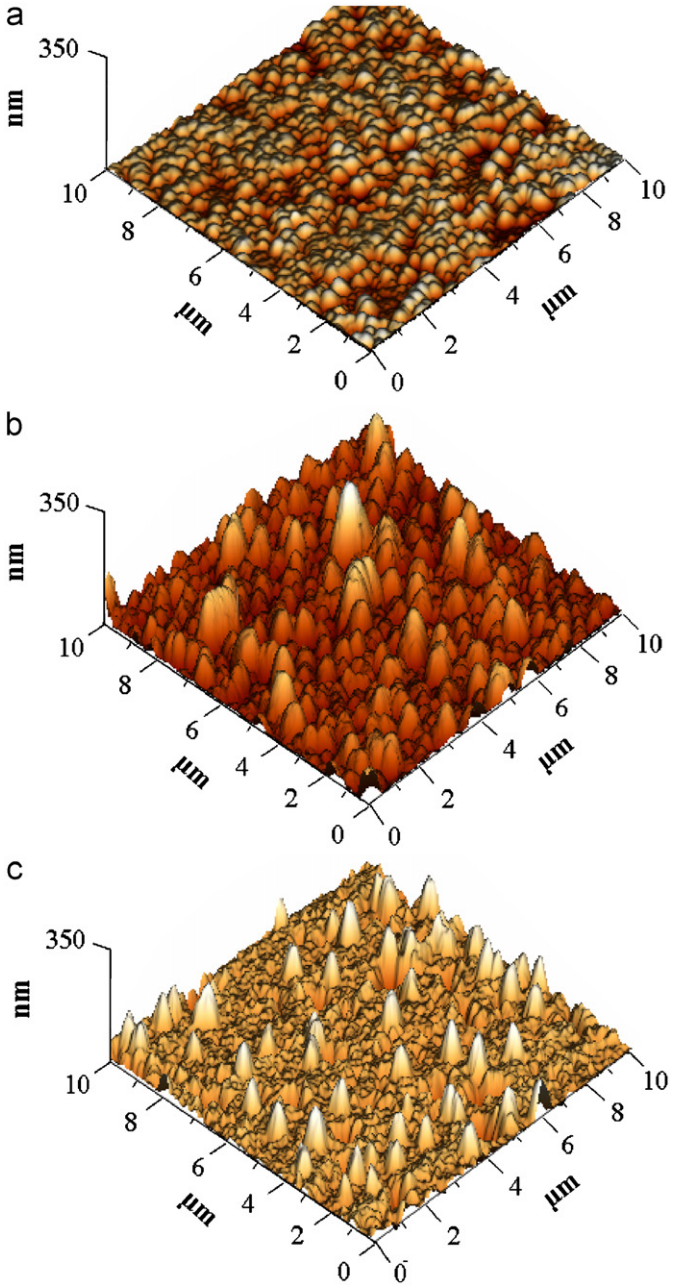

Fig. 2. Three-dimensional AFM images of the Ni nano-crystallised electrodeposits of 1 μm thickness on each of the investigated substrates: (a) Cu, (b) Au, and (c) ITO.

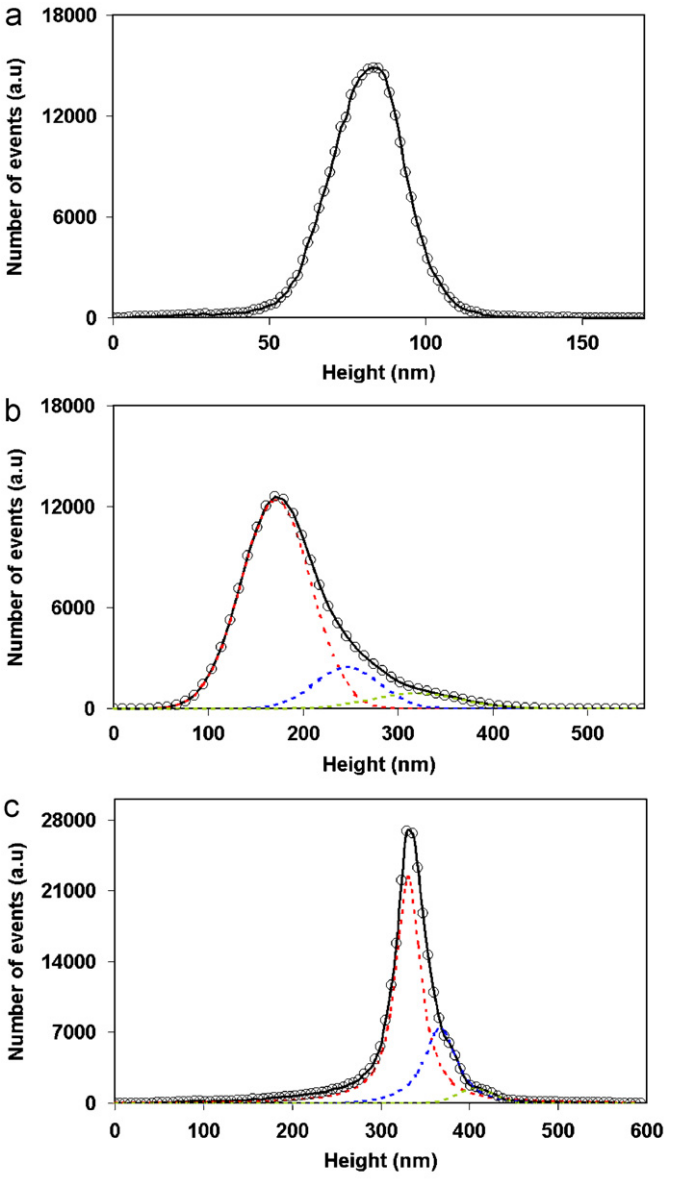

Fig. 3. Surface morphology histogram of the of the Ni nano-crystallised electrodeposits of 1 μm thickness on each of the investigated substrates: (a) Cu, (b) ITO, and (c) Au.

expected to obey the law

$$\sigma(L) = \frac{1}{N(L)} \left\{ \sum_{n=1}^{N} \sum_{m=1}^{N} [h(x_n, y_m) - \hbar]^2 \right\}^{1/2} \quad (1)$$

where $h(x, y)$ is the height at a pixel of the analysed area; N, the total number of pixels in this area; $\hbar$, the related average height value and L, the linear length or scale of the analysed area. Briefly, the spatial analysis, based on the scaling behaviour of σ=$f(L)$, leads one to evaluate the global roughness σ_{sat}, the correlation length, Lc and α the roughness exponent, while the dynamic analysis, based on the scaling behaviour of σ_{sat}=$f(t)$, with t the film deposition time, leads to evaluate the growth exponent β. We point out that the range of the investigated L and t regions of both σ=$f(L)$ and σ_{sat}=$f(t)$ curves covering some orders of magnitude as the required condition has been considered by many authors as relevant only for the computer-simulated analyses and is considered very ambitious for experimental results [15,16]. The spatial topography analysis of Ni films of 1 μm thick in Fig. 4 clearly shows that only the film grown on ITO (Fig. 4(b)) exhibits two linear features of the σ=$f(L)$ curves before the saturated zone, while Cu and Au both lead to a single linearity as illustrated in Fig. 4(a) for the case of Cu. We recently showed that the double linear feature of Ni film on ITO could be ascribed to the range of the J value applied [6,11], as only single linearity has been reported till now with the same substrate at quite low applied current density conditions [2,3]. The result of Ni film on Cu is in agreement with the trend observed previously with other transient elements electrodeposits, Co and Fe, on the same substrate [12]. To our knowledge, no topography result of Ni electrodeposits on Au substrate has been reported. Note that only the single linearity concurs with the classical theoretical

approach. For that purpose, the roughness exponents of the films on Cu (α_1=0.78) and Au (α_1=0.35) in Table 1 are both away from the typical 0.45 of the Kardar–Parizi–Zhang (KPZ) mode [15]. The double linear feature has been only recently examined in an updated KPZ approach [17,18]. The result with ITO does not match with the last model as the related α_1=0.71 deviates from the required $0.85 \leqslant \alpha_1 \leqslant 1$ range although α_2=0.21 is close to the good conditions. The topography factor defined as $k=\sigma_{sat}/Lc$ [13] clearly confirms the predominance of the vertical growth in every case, even with Cu substrate as its value always remains $k>1$. The important role of the nano-crystallites size should be underlined here for the film on Au as the topography factor k=5.04 and the mean grain height h''=400 nm have the highest values. On the other hand, the results of the film on ITO show that the relatively high nano-crystallite mean height h'=343 nm is associated with the lowest factor k=1.51. This is explained by the lowest nano-crystallites density appearing in Fig. 2(c). The better grain homogeneity of the film on Cu denotes that the topography reflects the absence of any particular morphology aspect. It should be underlined that the measured mean grain height is not sufficient to assess the film global roughness, σ_{sat}, that always remains less than 100 nm in agreement with the nano-crystallised characteristics of our Ni deposits. The dynamic scaling study of the film formation carried out as illustrated in Fig. 5 for the case of Ni–Cu system reveals a common linear feature leading to the growth exponents of Table 1. It appears here that this parameter is always $\beta \leqslant 0.50$, which is an indication of atomic diffusivity in both parallel and normal directions to the deposition substrate. This is engendered by both phenomena shadowing effect [15] and formation of a Schwoebel barrier [19].

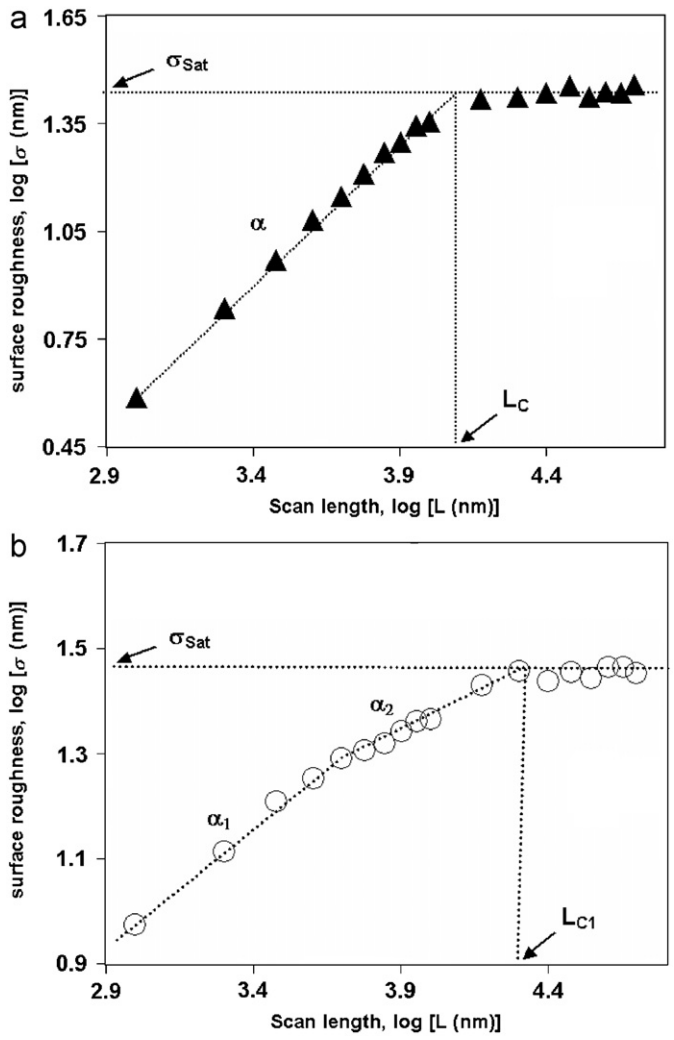

Fig. 4. Scaling feature of the surface roughness of the Ni nano-crystallised electrodeposits of 1 μm thickness on each one of the investigated substrates: (a) Cu and (b) ITO.

3.3. Transport properties of Ni ad-atoms in the film growth process

The topography histograms of the Ni samples of Fig. 3 clearly show that the major part of the investigated films consists of small grains although the entire film is dealt with in the study of the material transport properties on the deposition substrate. The theoretical approach used for that and developed in Ref. [6] is expressed through the following relation:

$$\frac{1}{\sigma_{sat}} = \left[3\left(\frac{2\gamma a^4 D_s}{\varepsilon_T}\right)^{1/4}\left(\frac{zF\rho}{\pi Mq}\right)\right] t^{1/4} \qquad (2)$$

where γ and ε_T, respectively, represent the interface and the thermal energies; a is the lattice parameter; D_s, the surface diffusion coefficient of the ad-atoms; z, the molar charge; F, the Faraday number; ρ, the material density; M, the molar mass; q, the charge density and t, the film deposition time. As explained elsewhere [6,7], the linearity of the equation $(1/\sigma_{sat})=f(t^{1/4})$ is the main condition to be fulfilled for the easy access to the surface

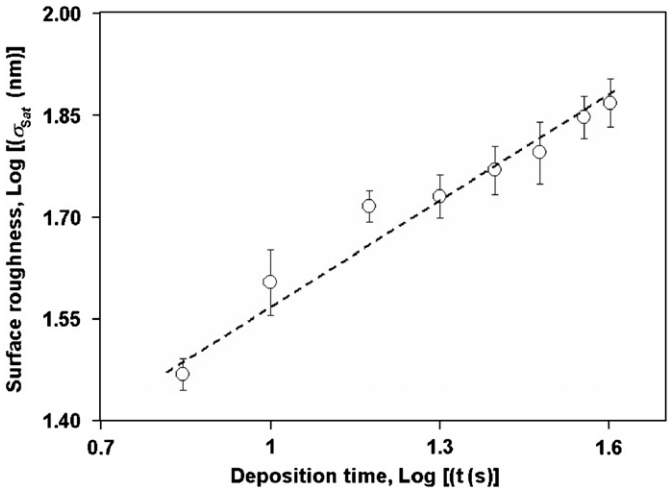

Fig. 5. Dependence of the saturated surface roughness on the film deposition time as obtained with Ni nano-crystallised electrodeposits grown on each of the investigated substrates illustrated here by the case of Ni films on Cu.

Table 1
Topography dependence of the Ni nano-structured films of 1 μm thick on the investigated deposition substrate materials.

Substrate material	Roughness exponent 1, α_1	Roughness exponent 2, α_2	Growth exponent β	Topography factor $K=\sigma_{sat}/Lc$ (a.u)
Cu	0.78 ± 0.01	–	0.51 ± 0.02	2.81
Au	0.32 ± 0.03	–	0.52 ± 0.01	5.04
ITO	0.71 ± 0.01	0.21 ± 0.02	0.67 ± 0.03	1.51

transport properties. This linearity leads to determination of the slope constant B corresponding to

$$B = 3\left(\frac{2\gamma a^4 D_s}{\varepsilon_T}\right)^{1/4}\left(\frac{zF\rho}{\pi Mq}\right) \quad (3)$$

From this is extracted the expression of the surface diffusion coefficient of the ad-atoms:

$$D_s = \frac{\varepsilon_T}{2\gamma a^4}\left(\frac{B\pi Mq}{3z\rho F}\right)^4 \quad (4)$$

The diffusion length, Λ_s, deduced from D_s through the Einstein relation is

$$\Lambda_s = (D_s\, t)^{1/2} \quad (5)$$

Plotting of Eq. (4) has been experimentally performed here with the following Ni characteristics: M(Ni)=58.71 g/mol; ρ(Ni)=8.30 g/cm^3; a(Ni)=3.524 × 10^{-8} cm; ε_T(Ni)=4.14 × 10^{-13} erg at the deposition temperature T=323 K; γ(Ni)=1700 erg/cm^2. The number of electrons transferred per Ni mole is z=2 here with q=0.05 C/cm^2 and F=96500 C/mol.

One points out that the proportionality between the reciprocal saturation roughness ($1/\sigma_{sat}$) and the time coefficient ($t^{1/4}$) of Eq. (2) can also be deduced from the dynamic analysis of the Family–Viscek theory. This clearly underlines the actual link between the topography and the transport characteristics of the material during the film formation. Experimentally, Nzoghe-Mendome [20] shown that the linearity of the $(1/\sigma_{sat})=f(t^{1/4})$ relation always occurs in a particular time interval preceeding a plateau. Besides, it has been showed that the extent of this interval is affected by the applied current density [8]. The results obtained here at J=22 mA cm^{-1} denote that the linearity of the $(1/\sigma_{sat})=f(t^{1/4})$ curves practically lies in the same time interval with all the investigated substrates, as illustrated in Fig. 6 for the case of Ni–Cu system. That linearity is a clear indication that the model used here for the study of the Ni film's surface transport properties is suitable. One can deduce from the slope values of Table 2 that these properties are directly induced by the substrate chemical nature as it is observed for the topography parameters. One can observe that Ni ad-atoms have very close D_s values on Cu (2.37×10^{-10} cm^2 s^{-1}) and ITO (3.41×10^{-10} cm^2 s^{-1}). This proximity remains worthy of further investigations. The higher diffusion coefficient (23.2×10^{-10} cm^2 s^{-1}) and diffusion length (37.32 nm) of the Ni–Au system confirm the particular effect of this substrate on the Ni ad-atoms motions. The D_s values of the present work are markedly higher than those evaluated in the range 10^{-16}–10^{-13} cm^2 s^{-1} for Au and Pt electrodeposits grown on polycrystalline substrates of the same materials [21]. Besides, the range 10^{-20}–10^{-16} cm^2 s^{-1} has been previously reported for their deposition in vacuum [22]. These examples evidence the crucial role of the deposition environment that determines the nature of the growth process to be taken into account for interpreting our surface transport results.

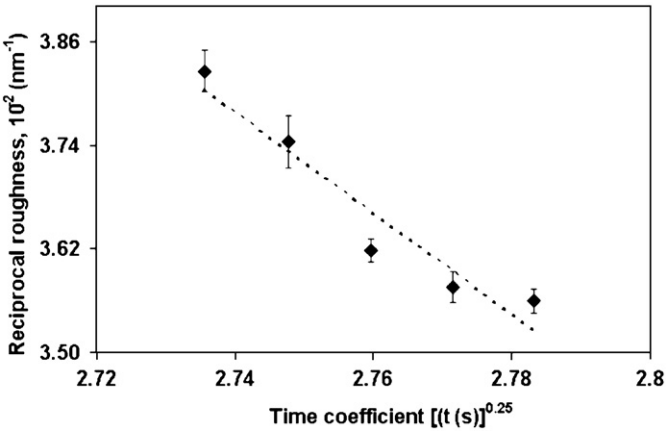

Fig. 6. Determination of the B constant (Eq. (3)) for the estimation of the Ni ad-atoms surface transport properties as obtained on each of the investigated substrates, illustrated here by the case of nano-crystallised Ni films on Cu.

Table 2
Surface transport properties dependence of Ni nano-structured films thick 1 μm on the investigated deposition substrate materials.

Substrate material	Slope constant of Eq. (5): B	Diffusion coefficient D_s (cm^2 s^{-1})	Diffusion length Λ_s (nm)
Cu	0.215	2.37×10^{-10}	11.92
Au	2.11	23.2×10^{-10}	37.32
ITO	0.31	3.41×10^{-10}	14.30

One observes that the lowest D_s values mostly result from a physical deposition whose growth process generally occurs under equilibrium conditions, at high temperatures [23]. The 10^{-16}–10^{-13} cm^2 s^{-1} values given above for Au and Pt electrodeposits could be ascribed to the experimental conditions closer to equilibrium as the related reduction of the oxide leading to metal overlayers is performed at extremely low-potential sweep rates. Consequently, the relatively high D_s values of the present work can be explained by the non-equilibrium conditions of the films deposition, stressed by the relatively high value of the applied current density.

4. Conclusion

The effects of the deposition substrate in the roughening and transport properties of Ni nano-crystallised electrodeposits are here identified. The vertical growth of big nano-crystallites and small grains obtained are clearly depicted. Their height repartition all over the film surface showed that Cu substrate gives rise to a mono-modal feature of moderate value. ITO leads to a tri-modal feature mainly depicting isolated big nano-crystallites located in the regions of small grains. The biggest particles grow on Au in a three-modal height feature. The model describing the link between topography and surface transport properties proposed concurs very well with the film deposition conditions as the measured sample's global roughness permits to establish the required linearity. The diffusion coefficients and lengths obtained are higher than those reported from pure physical deposition methods but they remain sufficiently consistent and lower than those of ion species in electrolytes.

This work shows that each Ni-substrate system can be separately explored for particular applications. The smoothness of Ni film on Cu is relevant for the interface charge transfer of device junctions while Ni on Au could be adequate for tribology. The particular surface feature of Ni on ITO favours the study of nano-dots fabrication in the cheapest way. Having in mind that these results only proceed from one current density of the deposition method, interesting features could be expected exploring many other deposition parameters in the same direction.

References

[1] Z. Petrovic, M. Metikos-Hukovic, Z. Grubac, S. Omanovic, Thin Solid Films 513 (2006) 193.
[2] M. Saitou, W. Oshikawa, A. Makabe, J. Phys. Chem. Sol. 63 (2002) 1685.

[3] M. Saitou, A. Makabe, T. Tomoyose, Surf. Sci. 459 (2000) L462.
[4] S. Sing, S. Basu, Surf. Coat. Technol. 201 (2006) 952.
[5] L. Nzoghe-Mendome, J. Ebothé, A. Aloufy, I.V. Kityk, J. Alloys Comp. 459 (2008) 232.
[6] M. Hiane, J. Ebothé, Eur. Phys. J. B 22 (2001) 485.
[7] L. Nzoghe-Mendome, A. Aloufy, J. Ebothé, D. Hui, M. El Messiry, Mater. Chem. Phys., in press.
[8] J.-L. Pouchou, Anal. Chem. Acta 283 (1993) 81.
[9] H. Benhayoune, N. Dumelié, G. Balossier, Thin Solid Film 493 (2005) 113.
[10] F. Family, T. Viscek, J. Phys. A 18 (1985) L75.
[11] Paul Meakin, Phys. Rep. 235 (1993) 189.
[12] J. Ebothé, S. Vilain, J. Phys. D: Appl. Phys. 32 (1999) 2342.
[13] J. Ebothé, A. El Hichou, P. Vautrot, M. Addou, J. Appl. Phys. 93 (2003) 632.
[14] A.L. Barabasi, H.E. Stanley, Fractal Concept in Surface Growth, Cambridge University Press, New York, 1995.
[15] S. Mendez, G. Andreasen, F. Schilardi, M. Figuerora, L. Vasquez, R.C. Salvarezza, A.J. Arvia, Langmuir 14 (1998) 2515.
[16] L. Vasquez, R.C. Salvarezza, P. Herrasti, P. Ocon, J.M. Vara, A.J. Arvia, Phys. Rev. B 52 (1995) 2032.
[17] T.J. Oliviera, F.D.A. Aarao Reis, J. Appl. Phys. 101 (2007) 063507.
[18] T. Paiva, F.D.A. Aarao Reis, Surf. Sci. 601 (2007) 419.
[19] R.L. Schwoebel, J. Appl. Phys. 40 (1968) 614.
[20] Leny Nzoghe-Mendome, PhD. Thesis, Université de Reims Champagne Ardenne, France, 2007.
[21] C. Alonso, R.C. Salvarezza, J.M. Vara, A.J. Arvia, L. Vazquez, A. Bartolome, A.M. Baro, J. Electrochem. Soc. 137 (1990) 2161.
[22] J. Schewers, R. Sonnenfeid, O. Marti, P.K. Hansma, J.E. Demuth, J. Harmers J. Appl. Phys. 63 (1988) 717.
[23] E. Bauer, Z. Kristallogr. 110 (1958) 372.